Proceedings of the
American Control Conference
Seattle, Washington • June 1995

A Benchmark Problem for Nonlinear Control Design: Problem Statement, Experimental Testbed, and Passive Nonlinear Compensation

Robert T. Bupp[1], Dennis S. Bernstein[1], and Vincent T. Coppola[2]
Department of Aerospace Engineering,
The University of Michigan
Ann Arbor, Michigan 48109

Abstract

This paper serves three distinct purposes. First, it provides the problem statement for the *Benchmark Problem for Nonlinear Control Design*, an invited session which is the basis for six related papers at this conference. The problem considers a translational oscillator with an attached eccentric rotational proof mass actuator, where the nonlinear coupling between the rotational motion of the actuator and the translational motion of the oscillator provides the mechanism for control. Secondly, the paper describes an experimental testbed that has been constructed by the authors to experimentally investigate this problem. Finally, the paper presents the authors' approach to the benchmark problem, which is based on the emulation of passive nonlinear mechanical absorbers with single and multiple modes. These controllers are shown to provide asymptotic stability and disturbance rejection with a bounded input signal. Both numerical and experimental results are presented.

1. Problem Statement

1.1. Introduction

In this section, we consider a nonlinear control design problem based on the nonlinear interaction of a translational oscillator and an attached rotational eccentric proof mass. This problem provides a benchmark for examining nonlinear control design techniques within the framework of a familiar spring-mass type system. The problem is in the spirit of the linear benchmark problem described in [1].

This system was originally proposed as a simplified model of a dual-spin spacecraft to investigate the resonance capture phenomenon [2]. It more recently has been studied to investigate the utility of a rotational proof mass actuator for stabilizing translational motion [3, 4]. Viewed in this setting, the rotational proof mass actuator has the feature that the nonlinearities associated with the stroke limitation are implicit in the system dynamics. In contrast, the stroke limitation issue must be considered separately in linear translational proof mass actuators [5].

1.2. Problem Statement

Consider the system shown in Fig. 1, which represents a translational oscillator with an eccentric rotational proof mass actuator. The oscillator consists of a cart of mass M

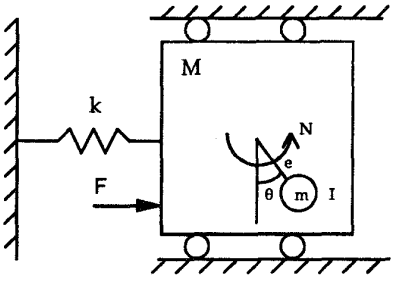

Figure 1: Translational Oscillator with Rotational Actuator

connected by a linear spring of stiffness k to a fixed wall. The cart is constrained to have one-dimensional travel. The proof mass actuator affixed to the cart has mass m and moment of inertia I about its center of mass. Its center of mass is located a distance e from the axis about which it rotates. We assume that the motion occurs in a horizontal plane, so that there are no gravitational forces to be considered. In Fig. 1, N denotes the control torque applied to the proof mass, and F is the disturbance force on the cart.

Let q and $\dot{q}$ denote the translational position and velocity of the cart, and let θ and $\dot{\theta}$ denote the angular position and velocity of the rotational proof mass. Then the equations of motion are given by

$$(M+m)\ddot{q} + kq = -me(\ddot{\theta}\cos\theta - \dot{\theta}^2\sin\theta) + F, \quad (1)$$

$$(I+me^2)\ddot{\theta} = -me\ddot{q}\cos\theta + N. \quad (2)$$

After suitable normalizations [3], the nondimensional equations of motion are given by

$$\ddot{\xi} + \xi = \varepsilon\left(\dot{\theta}^2\sin\theta - \ddot{\theta}\cos\theta\right) + w,$$

$$\ddot{\theta} = -\varepsilon\ddot{\xi}\cos\theta + u,$$

where w and u represent the nondimensionalized disturbance and torque, respectively. Note that the coupling between the translational and rotational motions is rep-

[1]Research supported in part by the Air Force Office of Scientific Research under Grant F49620-92-J-0127.
[2]Research supported in part by NSF Grant MSS-9309165.

resented by the parameter ϵ which is defined by

$$\epsilon \triangleq \frac{me}{\sqrt{(I+me^2)(M+m)}}. \tag{3}$$

Letting $x = [x_1, x_2, x_3, x_4]^T = [\xi, \dot{\xi}, \theta, \dot{\theta}]^T$, the nondimensional equations of motion in first-order form are given by

$$\dot{x} = f(x) + g(x)u + d(x)w, \tag{4}$$

where

$$f(x) = \begin{bmatrix} x_2 \\ \frac{-x_1+\epsilon x_4^2 \sin x_3}{1-\epsilon^2 \cos^2 x_3} \\ x_4 \\ \frac{\epsilon \cos x_3 (x_1 - \epsilon x_4^2 \sin x_3)}{1-\epsilon^2 \cos^2 x_3} \end{bmatrix},$$

$$g(x) = \begin{bmatrix} 0 \\ \frac{-\epsilon \cos x_3}{1-\epsilon^2 \cos^2 x_3} \\ 0 \\ \frac{1}{1-\epsilon^2 \cos^2 x_3} \end{bmatrix}, \quad d(x) = \begin{bmatrix} 0 \\ \frac{1}{1-\epsilon^2 \cos^2 x_3} \\ 0 \\ \frac{-\epsilon \cos x_3}{1-\epsilon^2 \cos^2 x_3} \end{bmatrix}.$$

The nonlinear benchmark problem can now be stated as follows.

Nonlinear Benchmark Problem. Design a control law that satisfies the following criteria:

1. The closed-loop system is stable (e.g., locally or globally).
2. The closed-loop system exhibits good disturbance rejection compared to the uncontrolled oscillator.
3. The control effort should be reasonable (e.g., maximum torque).

The requirements for stabilization, disturbance rejection, and control effort are not precisely stated. Instead, each designer may interpret these issues individually. Additionally, each designer is welcome to impose additional constraints on the problem as desired, where such features serve to highlight the capabilities of the particular nonlinear control design.

2. Experimental Testbed

To assess the practicality and effectiveness of using a rotational proof mass actuator to suppress translational motion, the authors have constructed a Rotational/Translational ACtuator (RTAC) Experimental Demonstration, based on the system described in the problem statement.

To get a rough idea of the experimental setup, view Fig. 1 as a "top view" looking down on the system operating in a horizontal plane. The cart of mass M consists of a pair of transparent acrylic plates. The spring k is realized by 2 to 12 helical springs symmetrically mounted and pretensioned. The control torque N is implemented by a rotary motor, onto whose shaft is mounted an eccentric arm. Low friction one-dimensional motion is obtained by mounting the cart on an air slide. The disturbance force F has not yet been implemented. A drawing of the setup is shown in Fig. 2. The remainder of this section provides a more detailed description of the experimental setup, including hardware components, sensors and actuators, and control implementation.

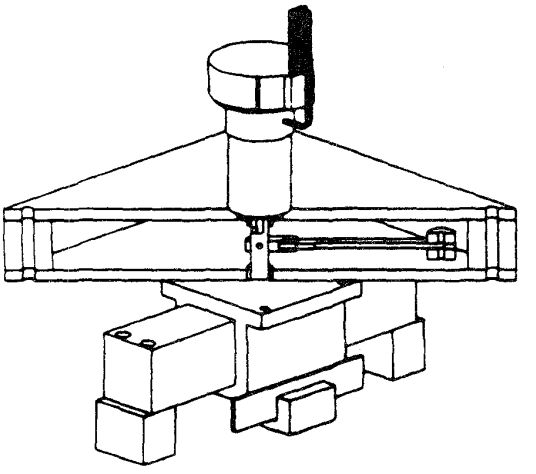

Figure 2: Drawing of the RTAC Experiment

The cart is constructed of two $8 \times 8 \times 0.25$ inch acrylic plates. The lower plate is bolted to a 3 inch long carriage, constrained to ride on the air slide, which has a usable length of 7 inches, thus allowing ± 2 inches travel. The upper plate is mounted directly above the lower plate on 1.125 inch acrylic mounting posts at the corners. The DC motor is mounted on the upper acrylic plate, with its shaft pointing downward. The total mass of the cart then consists of the sum of the masses of the acrylic plates, the mounting section of the air slide, the DC motor, and the mounting hardware, and is approximately 3 pounds. The natural frequency of the oscillator with 6 of the possible 12 springs attached is 1.8 Hz.

The eccentric arm connected to the motor shaft is a $4.25 \times .75 \times 0.0625$ inch aluminum bar, into which a 2.75 inch long slot is cut to facilitate mounting proof masses. The aluminum arm has a mass of 64 grams, and is scored at eighth-inch intervals to permit repeatability of the experimental configuration when proof masses are attached. The bar is fitted on a steel collar which is fastened with set screws to the motor shaft. While the eccentric arm alone serves as a rotational proof mass, we have constructed additional proof masses of steel which can be mounted to the eccentric arm at a range of locations. The additional proof masses are each $.75 \times .75 \times 0.0625$ inches, and weighs 4 grams. They can be stacked as many as six high and can be mounted on the arm between 1.5 and 3.25 inches from the motor shaft. With no proof masses attached to the arm, the value of the coupling parameter ϵ is roughly 0.2. The coupling increases as more mass is added.

The torque actuation is provided by a 12 volt Micro Mo *CR3557* DC brush motor that is 2.25 inches long and 1.38 inches in diameter. The motor produces 3.04 ounce-inches per amp, and is rated for continuous torque of 14.2 ounce-inches, and continuous power output of 45 watts. To achieve the torque ratings, the motor is capable of withstanding 4.67 amps continuous.

The angular position of the eccentric arm is sensed by an integral optical encoder mounted directly on the motor. The encoder has 1000 lines per revolution and two-channel quadrature output. The resulting angular resolution is 5.4 arcminutes or slightly less than 0.1 degree.

Since the encoder can operate at up to 200 kHz, the maximum angular rate at which the encoder will operate for this resolution is 200 Hz, well above the bandwidth of the system. To estimate angular velocity, we use a finite difference scheme on the angular position data.

Since we assume that our control input is torque, it follows that we should command the current into the motor. For this, we use a model 503 DC brushless servo drive from Copley Controls Corp. The pulse width modulated drive is rated to produce 5 amps continuous and 10 amps peak current with a bandwidth of 2.5 kHz.

In the first stages of the experiment, the translational position was measured by a linear optical encoder, and this sensor is depicted in the drawing of Fig. 2. However, while this sensor gave excellent data, the small amount of contact between the glass slide and the read head assembly caused excess friction in the system. In fact, the settling time for the uncontrolled system with the linear encoder in place was about 6 seconds for a one inch initial displacement, which corresponds to about 4 to 5 cycles. However, the settling time for the same initial condition with the encoder removed was in excess of one minute, the primary damping source in this case being the ambient air. Consequently, this sensor is being replaced with a noncontacting linear variable displacement transducer (LVDT).

The LVDT accepts ± 15 Volt DC input, and has a linear output range of ± 2 inches, which at 5.0 volts per inch yields a ± 10 Volt output. The output is rated linear to within 25 mV, or 5 mil. The LVDT consists of an 11.1 inch long stationary body that will be mounted to the table, and a 5.3 inch long core that will be mounted to the cart, and which will ride inside the body of the LVDT. To estimate translational velocity measurements, we will use a finite difference scheme. At the time this paper was written, the LVDT assembly and testing were incomplete.

To implement real-time control, we use a dSPACE ds1102 control board in conjunction with the dSPACE *Real Time Workshop* software which provides an interface to Matlab's *Simulink*. As a result, any control laws that can be represented by a *Simulink* block diagram, can be automatically converted to assembly code and implemented on the control board. This arrangement also allows for parameterized control laws, where the parameters can be adjusted on line, while the experiment is running.

The control board has two 12-bit A/D inputs plus two 16-bit A/D inputs, two encoder inputs, and four 12-bit D/A output ports. While the board is resident in a 90 MHz *Pentium*-based host PC, it utilizes its internal 40 MHz Texas Instruments TMS320C31 floating point digital signal processor for control.

3. Passive Nonlinear Compensation

Our initial objective for controller design is to asymptotically stabilize the system to the origin $q = \dot{q} = \theta = \dot{\theta} = 0$. This stability objective necessarily redefines the equilibrium structure of the system, since the equilibria of the open-loop system are $q = \dot{q} = \dot{\theta} = 0$, with arbitrary θ. We add the condition that the controller should not distinguish between the states $\theta \bmod 2\pi$ in general, and the states $\theta = 0 \bmod 2\pi$ in particular. We propose this additional condition because the states $\theta \bmod 2\pi$ represent equivalent physical configurations, and the inability of the controller to recognize this can result in undesirable *unwinding* behavior [6]. Finally, we add the condition that asymptotic stability must be global in the sense that all trajectories asymptotically approach the origin, $\bmod 2\pi$ in θ.

Our secondary objective in designing our controller is to provide disturbance rejection. We add the condition that the controller must have a preset torque bound, and of course must never compromise the primary stability objective. To achieve this secondary objective, we design compensators that emulate passive nonlinear dynamic vibration absorbers.

Our framework for controller synthesis described in [7], which is based on passivity notions. Central to this framework is the result that the negative feedback interconnection of a passive plant with a passive compensator is passive, and thus stable.

3.1. Damped Pendulum Absorber Emulation: Control Law Design

In this subsection, we are concerned with satisfying the primary objective of asymptotic stability of the idealized (frictionless) system. We note that the system described by equations (1), (2), with control input N and output

$$y = \dot{\theta}, \tag{5}$$

has an associated storage function

$$V_s(x) = \frac{1}{2}\Big[(M+m)\dot{q}^2 + kq^2 + (I+me^2)\dot{\theta}^2 + 2me\dot{q}\dot{\theta}\cos\theta\Big], \tag{6}$$

where $x = [\ q \quad \dot{q} \quad \theta \quad \dot{\theta}\ ]^{\mathrm{T}}$. The function $V_s(x)$ represents the kinetic and potential energy in the system. However, because of the rigid body rotational mode, $V_s(x)$ is nonnegative definite, but not positive definite, and the origin of the system is not Lyapunov stable. Furthermore, this system is not zero-state detectable, since $N \equiv 0$, $y \equiv 0$ does not imply $x \equiv 0$.

Our control design proceeds in two stages. First we design a control law $N = N_1(x)$ that ensures the closed-loop system is zero-state detectable. This renders the system passive, with an associated positive-definite storage function, and the closed-loop is then necessarily Lyapunov stable. Next, we design a passive controller $N_2(y)$ to achieve asymptotic stability. The final control law has the form

$$N = N_1(x) - N_2(y). \tag{7}$$

We first design a control law that will render this system zero-state detectable. Note that from (1), (2), (5) it follows that the conditions $N \equiv 0$, $y \equiv 0$ imply $\dot{q} \equiv 0$ and either

$$(M+m)\ddot{q} + kq = 0, \qquad \cos\theta \equiv 0, \tag{8}$$

or

$$q = \dot{q} = 0, \qquad \theta \text{ arbitrary}, \tag{9}$$

which are the undetectable modes.

To remove the undetectable modes, consider the control law

$$N_1(x) = -mge\sin\theta, \tag{10}$$

where $g > 0$, which is a bounded function of θ, and which has the desirable feature of not distinguishing between the values of $\theta \bmod 2\pi$, thereby avoiding the unwinding phenomenon.

The term $-mge\sin\theta$ lends itself to the interpretation of the gravitational torque that would result if the eccentric arm were in a gravitational field of strength g oriented in the $\theta = 0$ direction. Consequently, the controller can be interpreted as the active emulation of a damped pendulum absorber, which has been well studied in the literature for vibration suppression, for example [8]. Tuning of the emulated absorber can be accomplished by adjusting the value of the "gravitational" constant g, and by adjusting the damping parameter α.

The system (1), (2), (7), (10) with control input $N_2(y)$ and output $\dot{\theta}$ is passive with respect to the storage function

$$\bar{V}_s(x) = V_s(x) + mge(1 - \cos\theta), \tag{11}$$

which represents the original system energy plus the potential function from which the control law (10) was derived. Furthermore, the origin of the system is Lyapunov stabilized with bounded torque, and the system will not suffer unwinding. This system has Lyapunov stable equilibria at $q = \dot{q} = \dot{\theta} = 0$, $\theta = 0 \bmod 2\pi$, and unstable equilibria at $q = \dot{q} = \dot{\theta} = 0$, $\theta = \pi \bmod 2\pi$, which is not suprising since the controller emulates a pendulum absorber.

The control law $N_2(y) = \alpha\tanh(\gamma\dot{\theta})$, $\alpha,\ \gamma > 0$, which can be shown to be passive, yields [6]

$$N = -mge\sin\theta - \alpha\tanh(\gamma\dot{\theta}). \tag{12}$$

The closed-loop system has the form

$$(M+m)\ddot{q} + kq = -me(\ddot{\theta}\cos\theta - \dot{\theta}^2\sin\theta) + F, \tag{13}$$

$$(I + me^2)\ddot{\theta} = -me\ddot{q}\cos\theta - \alpha\dot{\theta} - mge\sin\theta. \tag{14}$$

Asymptotic stability of the closed-loop system (1), (2), (12) can be shown by considering the positive-definite Lyapunov function $\bar{V}_s(x)$. The rate of change of $\bar{V}_s(x)$ along the system trajectories is given by $\dot{\bar{V}}_s(x) = -\alpha\dot{\theta}\tanh(\gamma\dot{\theta})$. It follows from (13), (14) that the only trajectories that can remain on $\dot{\theta} = 0$ for a finite time are of the form $q = \dot{q} = \dot{\theta} = 0$, $\theta = 0 \bmod \pi$. It follows then that from every initial condition, the system trajectory will approach an equilibrium position. Note that with probability zero, an arbitrary trajectory will asymptotically approach an unstable equilibrium. However, a small disturbance will then cause the trajectory to asymptotically approach a stable equilibrium position $q = \dot{q} = \dot{\theta} = 0$, $\theta = 0 \bmod 2\pi$.

Let $N_{\max} > mge > 0$. Then $|N(x)| \le N_{\max}$, $x \in \mathbb{R}^4$. By choosing $\alpha = N_{\max} - mge > 0$, the closed-loop system is asymptotically stable, and the control torque never exceeds $N_{\max}$. Furthermore, $N_{\max}$ can be made arbitrarily small by a suitably small choice of g. Therefore, the control law (12) has asymptotically stabilized (1), (2), with arbitrarily small torque, and every closed-loop trajectory asymptotically approaches an equilibrium position $q = \dot{q} = \dot{\theta} = 0$, $\theta = 0 \bmod \pi$.

It should be noted that the linearization of the control law (12), given by

$$N = -mge\theta - \alpha\gamma\dot{\theta}, \tag{15}$$

will globally asymptotically stabilize the system in the conventional sense. However, there are two main drawbacks to this control. First, because the control law is linear, the control force is an unbounded function of the states θ and $\dot{\theta}$. Second while the linear control law produces exactly one globally asymptotically stable equilibrium at $x = 0$, it distinguishes between the states $\theta \bmod 2\pi$, and thus it suffers from unwinding. To see this, consider the initial condition $x = \dot{x} = \dot{\theta} = 0$, $\theta = 2M\pi$, for a very large integer M, and note that this initial condition is an equilibrium position of both the open-loop system, and the system with the control law (12). With (15), the closed-loop system will expend a great deal of effort to despin the eccentric arm M revolutions, possibly inducing large amplitude oscillations in q, finally to arrive at the origin, which is the same physical configuration as the initial condition.

The control law (12) was implemented on the RTAC Experimental Demsonstration described in the previous section. Figure 3.1 shows the open-loop (dashed) and closed-loop (solid) response to an initial cart displacement of about 1 inch. The upper plot shows the time history of

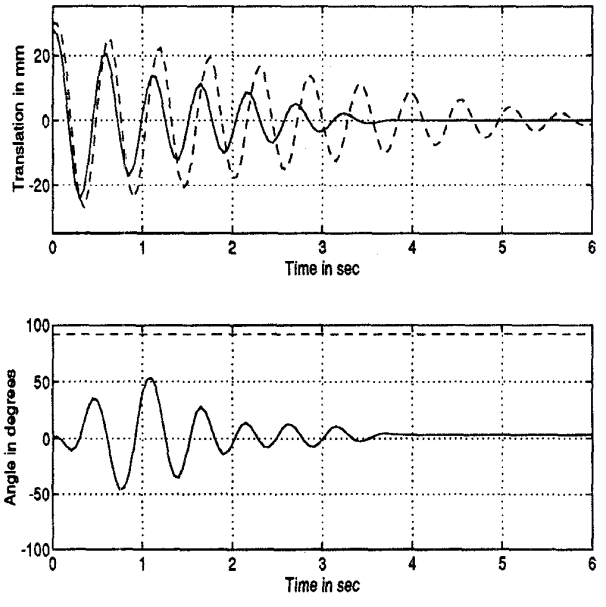

Figure 3: Experimental Open and Closed-Loop Response to 1 in. Initial Displacement

the cart displacement, and the lower plot shows the time history of the displacement of the proof mass actuator. As discussed in the previous section, a significant amount of damping in the translational encoder is evident in the decay rate of the open-loop system response.

Since the control law (12) does not require translational measurements, the experiment was also run with the encoder removed. In this case, the open-loop settling time was approximately 64 seconds, and the closed-loop settling time was reduced to approximately 6 seconds. How-

ever, due to the removal of the translational position sensor, the time history of the cart displacement was not measured.

So that we may better reject persistent disturbances at multiple frequencies, we are interested in designing dynamic compensators with multiple modes. In particular, we consider emulating coupled pendula.

3.2. Coupled Pendula Absorber Emulation: Compensator Design

In the previous subsection, we designed a control law to make the eccentric rotational proof mass actuator emulate a damped pendulum absorber. For the purpose of enhanced disturbance rejection, in this subsection we extend that design to the emulation of an absorber comprised of a system of coupled pendula. The stability properties of the damped pendulum absorber system are retained.

Recall from the previous subsection that the system (1), (2), (7), (10) with output $y = \dot{\theta}$ and control input N_2 is passive, with associated storage function $\bar{V}_s(x) = V_s(x) + mge(1 - \cos\theta)$. By designing a passive compensator with input $y = \dot{\theta}$ and output $N_c = -N_2$, the closed-loop system is guaranteed to be at least Lyapunov stable (see [7]). Our passive compensator is the emulation of the coupled pendula absorber in Fig. 4.

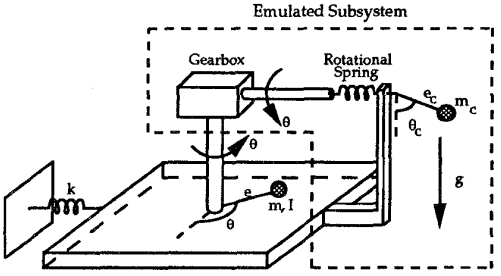

Figure 4: Coupled Pendula Absorber

The first pendulum in the figure is the eccentric proof mass actuator. While it is oriented in the horizontal plane, the control law (10) causes it to behave as if it were in a gravitational field of strength g. The angular motion of the first pendulum is transmitted up a rigid rod and through a gear box to a second rigid rod. The angular motion of the two rods follow exactly the angular motion of the eccentric arm. The horizontal rod connects to the second pendulum by a rotational spring/damper element. The second pendulum then hangs vertically in the gravitational field. Since the angular motion of the second pendulum is normal to the motion of the cart, the pendulum does not couple with the translational motion as the eccentric arm does.

Since the first pendulum is represented by the eccentric arm of the proof mass actuator, it has mass m, centroidal inertia I, eccentricity e, and absolute angle θ as defined previously. The second pendulum is defined by a point mass m_c at a distance e_c about the rotational axis, with absolute angle θ_c. The pendula are connected by a nonlinear elastic coupling with restoring torque $\pm\kappa\sin(\theta-\theta_c)$ where $\kappa > 0$, and the minus sign in the expression is associated with the restoring torque at the first pendulum, while the plus sign is associated with the restoring torque at the second pendulum. The control torque is denoted N_c.

To realize the compensator that emulates the coupled pendula absorber in Fig. 4, we write the equations of motion with input $y = \theta$, and output $N_c = -N_2$. These equations are given by

$$\dot{x}_c = f_c(x_c) + G_c(x_c, y)y, \tag{16}$$

$$N_c = h_c(x_c, y) + J_c(x_c, y)y, \tag{17}$$

where $x_c = [\ \theta \quad \theta_c \quad \dot{\theta}_c\ ]^T$, and

$$f_c(x_c) = \begin{bmatrix} 0 \\ \dot{\theta}_c \\ -\frac{\sin(\theta_c-\theta)}{(m_c e_c^2)} - \frac{g\sin\theta_c}{e_c} \end{bmatrix}, \quad G_c(x_c, y) = \begin{bmatrix} 1 \\ 0 \\ 0 \end{bmatrix},$$

$$h_c(x_c, y) = \kappa\sin(\theta - \theta_c), \quad J_c(x_c, y) = \frac{\alpha\tanh(\gamma y)}{y}.$$

This compensator is passive, with the associated storage function

$$V_{sc}(x_c) = \tfrac{1}{2}m_c e_c^2\dot{\theta}_c^2 + m_c g e_c(1 - \cos\theta_c) + \kappa(1 - \cos(\theta - \theta_c)). \tag{18}$$

It is straightforward to show that the equilibria and their stability properties are precisely as they were in the previous subsection, with the control law (12). By emulating the additional virtual pendulum coupled to the first, we have produced a compensator that is sensitive to multiple disturbance frequencies, and therefore may be better able to reject disturbances near these frequencies.

References

[1] B. Wie and D. S. Bernstein. Benchmark problems in robust control design. *Journal of Guidance, Control and Dynamics*, Vol. 15, pp. 1057 – 1059, 1992.

[2] R. H. Rand, R. J. Kinsey, and D. L. Mingori. Dynamics of spinup through resonance. *International Journal of Non-Linear Mechanics*, Vol. 27, No. 3, pp. 489–502, 1992.

[3] C. J. Wan, D. S. Bernstein, and V. T. Coppola. Global stabilization of the oscillating eccentric rotor. In *Proc. IEEE Conf. Dec. Contr.*, pp. 4024 – 4029, Orlando, FL, 1994.

[4] R. T. Bupp, V. T. Coppola, and D. S. Bernstein. Vibration suppression of multi-modal translational motion using a rotational actuator. In *Proc. IEEE Conf. Dec. Contr.*, pp. 4030 – 4034, Orlando, FL, 1994.

[5] D. K. Lindner, T. P. Celano, and E. N. Ide. Vibration suppression using a proofmass actuator operating in stroke/force saturation. *Journal of Vibrations and Acoustics*, Vol. 113, pp. 423–433, 1991.

[6] R. T. Bupp, C. J. Wan, V. T. Coppola, and D. S. Bernstein. Design of a rotational actuator for global stabilization of translational motion. In *Proc. ASME Winter Meeting, DE-Vol 75*, pp. 449 – 456, Chicago, IL, 1994.

[7] R. T. Bupp, J. R. Corrado, V. T. Coppola, and D. S. Bernstein. Nonlinear modification of positive-real LQG compensators for enhanced disturbance rejection and energy dissipation. In *Proc. ACC*, Seattle, WA, 1995.

[8] B. G. Korenov and L. M. Reznikov. *Dynamic Vibration Absorbers: Theory and Technical Applications*. Wiley, 1993.